InN-based heterojunction photodetector with extended infrared response

Lung-Hsing Hsu,[1] Chien-Ting Kuo,[1] Jhih-Kai Huang,[2] Shun-Chieh Hsu,[3] Hsin-Ying Lee,[4] Hao-Chung Kuo,[2] Po-Tsung Lee,[2] Yu-Lin Tsai,[2] Yi-Chia Hwang,[3] Chen-Feng Su,[3] Jr-Hau He,[5] Shih-Yen Lin,[6] Yuh-Jen Cheng,[6] and Chien-Chung Lin[3,*]

[1]Institute of Lighting and Energy Photonics, National Chiao Tung University, Tainan 71150, Taiwan
[2]Institute of Electro-Optical Engineering, National Chiao Tung University, Hsinchu 30010, Taiwan
[3]Institute of Photonic System, National Chiao Tung University, Tainan 71150, Taiwan
[4]Department of Photonics, National Cheng Kung University, Tainan 70101, Taiwan
[5]Computer, Electrical and Mathematical Sciences and Engineering (CEMSE) Division, King Abdullah University of Science & Technology (KAUST), Thuwal 23955-6900, Saudi Arabia
[6]Research Center for Applied Sciences, Academia Sinica, Taiwan
[*] chienchunglin@faculty.nctu.edu.tw

Abstract: The combination of ZnO, InN, and GaN epitaxial layers is explored to provide long wavelength photodetection capability in the GaN based materials. Growth temperature optimization was performed to obtain the best quality of InN epitaxial layer in the MOCVD system. The temperature dependent photoluminescence (PL) can provide the information about thermal quenching in the InN PL transitions and at least two non-radiative processes can be observed. X-ray diffraction and energy dispersive spectroscopy are applied to confirm the inclusion of indium and the formation of InN layer. The band alignment of such system shows a typical double heterojunction, which is preferred in optoelectronic device operation. The photodetector manufactured by this ZnO/GaN/InN layer can exhibit extended long-wavelength quantum efficiency, as high as 3.55%, and very strong photocurrent response under solar simulator illumination.

OCIS codes: (040.5160) Photodetectors; (160.6000) Semiconductor materials; (250.5230) Photoluminescence; (310.6188) Spectral properties; (040.3060) Infrared.

References and links

1. E. F. Schubert, *Light Emitting Diodes*, 2nd ed. (Cambridge, U.K.: Cambridge Univ. Press, 2003).
2. C. H. Chiu, P. M. Tu, C. C. Lin, D. W. Lin, Z. Y. Li, K. L. Chuang, J. R. Chang, T. C. Lu, H. W. Zan, C. Y. Chen, H. C. Kuo, S. C. Wang, and C. Y. Chang, "Highly Efficient and Bright LEDs Overgrown on GaN Nanopillar Substrates," IEEE J. Sel. Top. Quantum Electron. **17**(4), 971–978 (2011).
3. S. Nakamura, S. Pearton, and G. Fasol, *The Blue Laser Diode*, 2nd ed. (Berlin, Germany: Springer-Verlag, 2000).
4. S. Nakamura, M. Senoh, S. Nagahama, N. Iwasa, T. Yamada, T. Matsushita, H. Kiyoku, Y. Sugimoto, T. Kozaki, H. Umemoto, M. Sano, and K. Chocho, "InGaN/GaN/AlGaN-based laser diodes with modulation-doped strained-layer superlattices grown on an epitaxially laterally overgrown GaN substrate," Appl. Phys. Lett. **72**(2), 211–213 (1998).
5. C.-C. Chen, C.-H. Chiu, P.-M. Tu, M.-Y. Kuo, M. H. Shih, J.-K. Huang, H.-C. Kuo, H.-W. Zan, and C.-Y. Chang, "Large Area of Ultraviolet GaN-Based Photonic Quasicrystal Laser," Jpn. J. Appl. Phys. **51**(4S), 04DG02 (2012).
6. C. J. Neufeld, N. G. Toledo, S. C. Cruz, M. Iza, S. P. DenBaars, and U. K. Mishra, "High quantum efficiency InGaN/GaN solar cells with 2.95 eV band gap," Appl. Phys. Lett. **93**(14), 143502 (2008).
7. Y.-L. Tsai, C.-C. Lin, H.-V. Han, C.-K. Chang, H.-C. Chen, K.-J. Chen, W.-C. Lai, J.-K. Sheu, F.-I. Lai, P. Yu, and H.-C. Kuo, "Improving efficiency of InGaN/GaN multiple quantum well solar cells using CdS quantum dots and distributed Bragg reflectors," Sol. Energy Mater. Sol. Cells **117**, 531–536 (2013).
8. H. W. Wang, H. C. Chen, Y. A. Chang, C. C. Lin, H. W. Han, M. A. Tsai, H. C. Kuo, P. Yu, and S. H. Lin, "Conversion Efficiency Enhancement of GaN/$In_{0.11}Ga_{0.89}N$ Solar Cells With Nano Patterned Sapphire and Biomimetic Surface Antireflection Process," IEEE Photonics Technol. Lett. **23**(18), 1304–1306 (2011).
9. L.-H. Hsu, C.-C. Lin, H.-V. Han, D.-W. Lin, Y.-H. Lo, Y.-C. Hwang, and H.-C. Kuo, "Enhanced photocurrent of a nitride-based photodetector with InN dot-like structures," Opt. Mater. Express **4**(12), 2565–2573 (2014).
10. A. Winden, M. Mikulics, A. Haab, D. Grützmacher, and H. Hardtdegen, "Spectral Sensitivity Tuning of Vertical InN Nanopyramid-Based Photodetectors," Jpn. J. Appl. Phys. **52**(8S), 08JF05 (2013).

#249488 Received 4 Sep 2015; revised 7 Nov 2015; accepted 16 Nov 2015; published 20 Nov 2015

11. K. You, H. Jiang, D. Li, X. Sun, H. Song, Y. Chen, Z. Li, G. Miao, and H. Liu, "Shift of responsive peak in GaN-based metal-insulator-semiconductor photodetectors," Appl. Phys. Lett. **100**(12), 121109 (2012).
12. C.-H. Chen, K.-R. Wang, S.-Y. Tsai, H.-J. Chien, and S.-L. Wu, "Nitride-Based Metal–Semiconductor–Metal Photodetectors with InN/GaN Multiple Nucleation Layers," Jpn. J. Appl. Phys. **49**(4), 04DG06 (2010).
13. J. Wu, "When group-III nitrides go infrared: New properties and perspectives," J. Appl. Phys. **106**(1), 011101 (2009).
14. J. Wu, W. Walukiewicz, W. Shan, K. M. Yu, J. W. Ager, S. X. Li, E. E. Haller, H. Lu, and W. J. Schaff, "Temperature dependence of the fundamental band gap of InN," J. Appl. Phys. **94**(7), 4457 (2003).
15. T. Matsuoka, H. Okamoto, M. Nakao, H. Harima, and E. Kurimoto, "Optical bandgap energy of wurtzite InN," Appl. Phys. Lett. **81**(7), 1246 (2002).
16. A. G. Bhuiyan, A. Hashimoto, and A. Yamamoto, "Indium nitride (InN): A review on growth, characterization, and properties," J. Appl. Phys. **94**(5), 2779 (2003).
17. K. M. Yu, Z. Liliental-Weber, W. Walukiewicz, W. Shan, J. W. Ager, S. X. Li, R. E. Jones, E. E. Haller, H. Lu, and W. J. Schaff, "On the crystalline structure, stoichiometry and band gap of InN thin films," Appl. Phys. Lett. **86**(7), 071910 (2005).
18. J. Park, H. Ryu, T. Son, and S. Yeon, "Epitaxial Growth of ZnO/InN Core/Shell Nanostructures for Solar Cell Applications," Appl. Phys. Express **5**(10), 101201 (2012).
19. B. H. Le, S. Zhao, N. H. Tran, and Z. Mi, "Electrically injected near-infrared light emission from single InN nanowire p-i-n diode," Appl. Phys. Lett. **105**(23), 231124 (2014).
20. H. P. T. Nguyen, Y. L. Chang, I. Shih, and Z. Mi, "InN p-i-n Nanowire Solar Cells on Si," IEEE J. Sel. Top. Quantum Electron. **17**(4), 1062–1069 (2011).
21. W. Huang, M. Yoshimoto, K. Taguchi, H. Harima, and J. Saraie, "Improved Electrical Properties of InN by High-Temperature Annealing with In Situ Capped SiNx Layers," Jpn. J. Appl. Phys. **43**(1A/B), L97–L99 (2004).
22. T. Fujii, A. Kobayashi, K. Shimomoto, J. Ohta, M. Oshima, and H. Fujioka, "Structural Characteristics of GaN/InN Heterointerfaces Fabricated at Low Temperatures by Pulsed Laser Deposition," Appl. Phys. Express **3**(2), 021003 (2010).
23. R. E. Jones, K. M. Yu, S. X. Li, W. Walukiewicz, J. W. Ager, E. E. Haller, H. Lu, and W. J. Schaff, "Evidence for p-Type Doping of InN," Phys. Rev. Lett. **96**(12), 125505 (2006).
24. S. Zhao, X. Liu, and Z. Mi, "Photoluminescence properties of Mg-doped InN nanowires," Appl. Phys. Lett. **103**(20), 203113 (2013).
25. S. Zhao, B. H. Le, D. P. Liu, X. D. Liu, M. G. Kibria, T. Szkopek, H. Guo, and Z. Mi, "p-Type InN Nanowires," Nano Lett. **13**(11), 5509–5513 (2013).
26. N. P. Dasgupta, S. Neubert, W. Lee, O. Trejo, J.-R. Lee, and F. B. Prinz, "Atomic Layer Deposition of Al-doped ZnO Films: Effect of Grain Orientation on Conductivity," Chem. Mater. **22**(16), 4769–4775 (2010).
27. Y. K. Fu, C. H. Kuo, C. J. Tun, C. W. Kuo, W. C. Lai, G. C. Chi, C. J. Pan, M. C. Chen, H. F. Hong, and S. M. Lan, "Self-assembled InN dots grown on GaN with an $In_{0.08}Ga_{0.92}N$ intermediate layer by metal organic chemical vapor deposition," J. Cryst. Growth **310**(20), 4456–4459 (2008).
28. J. Kamimura, K. Kishino, and A. Kikuchi, "Growth of very large InN microcrystals by molecular beam epitaxy using epitaxial lateral overgrowth," J. Appl. Phys. **117**(8), 084314 (2015).
29. A. Vodopyanov, Y. Buzynin, D. Mansfeld, O. Khrykin, Y. Drozdov, P. Yunin, A. Lukyanov, M. Viktorov, S. Golubev, and V. Shashkin, "Monocrystalline InN Films Grown at High Rate by Organometallic Vapor Phase Epitaxy with Nitrogen Plasma Activation Supported by Gyrotron Radiation," Jpn. J. Appl. Phys. **52**(11R), 110201 (2013).
30. T. Iwabuchi, Y. Liu, T. Kimura, Y. Zhang, K. Prasertsuk, H. Watanabe, N. Usami, R. Katayama, and T. Matsuoka, "Effect of Phase Purity on Dislocation Density of Pressurized-Reactor Metalorganic Vapor Phase Epitaxy Grown InN," Jpn. J. Appl. Phys. **51**(4S), 04DH02 (2012).
31. Y. Pan, T. Wang, K. Shen, T. Peng, K. Wu, W. Zhang, and C. Liu, "Rapid growth and characterization of InN nanocolumns on InGaN buffer layers at a low ratio of N/In," J. Cryst. Growth **313**(1), 16–19 (2010).
32. J. Sakaguchi, T. Araki, T. Fujishima, E. Matioli, T. Palacios, and Y. Nanishi, "Thickness Dependence of Structural and Electrical Properties of Thin InN Grown by Radio-Frequency Plasma-Assisted Molecular Beam Epitaxy," Jpn. J. Appl. Phys. **52**(8S), 08JD06 (2013).
33. W. C. Chen, Y. H. Tian, Y.-H. Wu, W.-L. Wang, S.-Y. Kuo, F.-I. Lai, and L. Chang, "Influence of V/III Flow Ratio on Growth of InN on GaN by PA-MOMBE," J. Solid State Sci. Technol. **2**(7), P305–P310 (2013).
34. B. N. Pantha, R. Dahal, M. L. Nakarmi, N. Nepal, J. Li, J. Y. Lin, H. X. Jiang, Q. S. Paduano, and D. Weyburne, "Correlation between optoelectronic and structural properties and epilayer thickness of AlN," Appl. Phys. Lett. **90**(24), 241101 (2007).
35. R. Chierchia, T. Böttcher, H. Heinke, S. Einfeldt, S. Figge, and D. Hommel, "Microstructure of heteroepitaxial GaN revealed by x-ray diffraction," J. Appl. Phys. **93**(11), 8918–8925 (2003).
36. W. C. Ke, C. P. Fu, C. Y. Chen, L. Lee, C. S. Ku, W. C. Chou, W.-H. Chang, M. C. Lee, W. K. Chen, W. J. Lin, and Y. C. Cheng, "Photoluminescence properties of self-assembled InN dots embedded in GaN grown by metal organic vapor phase epitaxy," Appl. Phys. Lett. **88**(19), 191913 (2006).
37. N. Hong Tran, B. Huy Le, S. Fan, S. Zhao, Z. Mi, B. A. Schmidt, M. Savard, G. Gervais, and K. S. A. Butcher, "Optical and structural characterization of nitrogen-rich InN: Transition from nearly intrinsic to strongly n-type degenerate with temperature," Appl. Phys. Lett. **103**(26), 262101 (2013).
38. J. Segura-Ruiz, N. Garro, A. Cantarero, C. Denker, J. Malindretos, and A. Rizzi, "Optical studies of MBE-grown InN nanocolumns: Evidence of surface electron accumulation," Phys. Rev. B **79**(11), 115305 (2009).
39. A. A. Klochikhin, V. Y. Davydov, V. V. Emtsev, A. V. Sakharov, V. A. Kapitonov, B. A. Andreev, H. Lu, and W. J. Schaff, "Acceptor states in the photoluminescence spectra of n-InN," Phys. Rev. B **71**(19), 195207 (2005).

#249488 Received 4 Sep 2015; revised 7 Nov 2015; accepted 16 Nov 2015; published 20 Nov 2015

40. M. Leroux, N. Grandjean, B. Beaumont, G. Nataf, F. Semond, J. Massies, and P. Gibart, "Temperature quenching of photoluminescence intensities in undoped and doped GaN," J. Appl. Phys. **86**(7), 3721–3728 (1999).
41. C.-L. Hsiao, H.-C. Hsu, L.-C. Chen, C.-T. Wu, C.-W. Chen, M. Chen, L.-W. Tu, and K.-H. Chen, "Photoluminescence spectroscopy of nearly defect-free InN microcrystals exhibiting nondegenerate semiconductor behaviors," Appl. Phys. Lett. **91**(18), 181912 (2007).
42. S. Chichibu, T. Sota, K. Wada, and S. Nakamura, "Exciton localization in InGaN quantum well devices," J. Vac. Sci. Technol. B **16**(4), 2204–2214 (1998).
43. C. Adelmann, J. Simon, G. Feuillet, N. T. Pelekanos, B. Daudin, and G. Fishman, "Self-assembled InGaN quantum dots grown by molecular-beam epitaxy," Appl. Phys. Lett. **76**(12), 1570 (2000).
44. B. Arnaudov, T. Paskova, P. P. Paskov, B. Magnusson, E. Valcheva, B. Monemar, H. Lu, W. J. Schaff, H. Amano, and I. Akasaki, "Energy position of near-band-edge emission spectra of InN epitaxial layers with different doping levels," Phys. Rev. B **69**(11), 115216 (2004).
45. J. D. Lambkin, L. Considine, S. Walsh, G. M. O'Connor, C. J. McDonagh, and T. J. Glynn, "Temperature dependence of the photoluminescence intensity of ordered and disordered $In_{0.48}Ga_{0.52}P$," Appl. Phys. Lett. **65**(1), 73–75 (1994).
46. M. Gurioli, J. Martinez-Pastor, M. Colocci, C. Deparis, B. Chastaingt, and J. Massies, "Thermal escape of carriers out of GaAs/AlxGa1-xAs quantum-well structures," Phys. Rev. B Condens. Matter **46**(11), 6922–6927 (1992).
47. S. Marcinkevičius, K. M. Kelchner, L. Y. Kuritzky, S. Nakamura, S. P. DenBaars, and J. S. Speck, "Photoexcited carrier recombination in wide m-plane InGaN/GaN quantum wells," Appl. Phys. Lett. **103**(11), 111107 (2013).
48. Y. Huang, K. W. Sun, A. M. Fischer, Q. Y. Wei, R. Juday, F. A. Ponce, R. Kato, and T. Yokogawa, "Effect of misfit dislocations on luminescence in m-plane InGaN quantum wells," Appl. Phys. Lett. **98**(26), 261914 (2011).
49. D. W. Jenkins and J. D. Dow, "Electronic structures and doping of InN, $In_xGa_{1-x}N$, and $In_xAl_{1-x}N$," Phys. Rev. B Condens. Matter **39**(5), 3317–3329 (1989).
50. X. M. Duan and C. Stampfl, "Vacancies and interstitials in indium nitride: Vacancy clustering and molecular bondlike formation from first principles," Phys. Rev. B **79**(17), 174202 (2009).
51. G. W. Shu, P. F. Wu, M. H. Lo, J. L. Shen, T. Y. Lin, H. J. Chang, Y. F. Chen, C. F. Shih, C. A. Chang, and N. C. Chen, "Concentration dependence of carrier localization in InN epilayers," Appl. Phys. Lett. **89**(13), 131913 (2006).
52. M. Feneberg, J. Däubler, K. Thonke, R. Sauer, P. Schley, and R. Goldhahn, "Mahan excitons in degenerate wurtzite InN: Photoluminescence spectroscopy and reflectivity measurements," Phys. Rev. B **77**(24), 245207 (2008).
53. P.-C. Wei, S. Chattopadhyay, F.-S. Lin, C.-M. Hsu, S. Jou, J.-T. Chen, P.-J. Huang, H.-C. Hsu, H.-C. Shih, K.-H. Chen, and L.-C. Chen, "Origin of the anomalous temperature evolution of photoluminescence peak energy in degenerate InN nanocolumns," Opt. Express **17**(14), 11690–11697 (2009).
54. S.-C. Shi, C.-F. Chen, G.-M. Hsu, J.-S. Hwang, S. Chattopadhyay, Z.-H. Lan, K.-H. Chen, and L.-C. Chen, "Reduced temperature-quenching of photoluminescence from indium nitride nanotips grown by metalorganic chemical vapor deposition," Appl. Phys. Lett. **87**(20), 203103 (2005).
55. X.-M. Zhang, M.-Y. Lu, Y. Zhang, L.-J. Chen, and Z. L. Wang, "Fabrication of a High-Brightness Blue-Light-Emitting Diode Using a ZnO-Nanowire Array Grown on p-GaN Thin Film," Adv. Mater. **21**(27), 2767–2770 (2009).
56. H. Zhu, C. X. Shan, B. Yao, B. H. Li, J. Y. Zhang, D. X. Zhao, D. Z. Shen, and X. W. Fan, "High Spectrum Selectivity Ultraviolet Photodetector Fabricated from an n-ZnO/p-GaN Heterojunction," J. Phys. Chem. C **112**(51), 20546–20548 (2008).
57. B. Roul, M. K. Rajpalke, T. N. Bhat, M. Kumar, N. Sinha, A. T. Kalghatgi, and S. B. Krupanidhi, "Temperature dependent electrical transport behavior of InN/GaN heterostructure based Schottky diodes," J. Appl. Phys. **109**(4), 044502 (2011).

1. Introduction

Recently, nitride–based alloys, such as AlN, GaN and InN, have achieved great success in the applications of optoelectronic devices such as light emitting diodes [1, 2], lasers [3–5], solar cells [6–8], and photodetectors [9–12]. One of the key features about this nitride-based materials is the direct bandgap energy covering from 0.7 eV (for InN) to 6.2 eV (for AlN), and thus provides wide range of absorption from ultraviolet to infrared [13–15]. While many research groups have worked on the GaN/AlN related materials, the narrow-band-gap InN represents a unique opportunity for extending the applicable wavelength into the traditionally important 1.3 to 1.5 μm range. However, most efforts in the past were focused on the growth mechanism and material characterization of InN [16–18] mainly due to the exotic growth condition and large lattice mismatch of InN to its substrate. One solution is to use molecular beam epitaxy (MBE), in which the substrate temperature can be controlled such that the incoming indium atoms can be deposited via surface chemical reaction, and great results in

#249488 Received 4 Sep 2015; revised 7 Nov 2015; accepted 16 Nov 2015; published 20 Nov 2015

light emitting diode and solar cells [19, 20] have been demonstrated. In a practical metal organic chemical vapor deposition (MOCVD) system, the growth temperature is often more than 800°C, which can be detrimental to the InN layer due to low evaporation point of indium [16]. Such limitation restrains the subsequent growth of the capping layer and thus affect the overall epitaxial layer design [21, 22]. Another obstacle rises from the high background electron concentration inherent for InN, so the p-type InN is difficult to achieve [23–25]. Without a proper capping layer or suitable p-InN material, the progress of InN related device could be hindered.

In this study, we employed a low-pressure MOCVD to grow a GaN/InN structures. To properly address the capping layer problem, a combination of low-temperature GaN (LT-GaN) and atomic-layer-deposition (ALD) ZnO layers is applied on top of the grown InN layer. Various growth conditions were explored, and material characterization were performed to reveal the best temperature for InN epitaxy. The extended InN absorption peak and photoluminescence peak shift phenomenon can be observed in both cryogenic and room temperature. Finally, this ZnO/LT-GaN/InN hetero-structure was manufactured into an infrared-ready photodetector with an external quantum efficiency as high as 3.55% at 1650 nm.

2. Experiments

The nitride related structure was grown on c-plane sapphire substrate by a low-pressure MOCVD. The epitaxial structure consists of (counting from the substrate and up): a 25-nm low-temperature GaN nucleation layer, a 1.5-μm undoped GaN (u-GaN) layer, a 1-μm Mg doped GaN layer (p-GaN), and a 65-nm InN layer. The 65-nm InN layer was grown under different temperatures varied from 510°C to 550°C. Finally, a 100-nm LT-GaN grown at the same temperature as the InN's was used to cap the overall structure. During the growth, trimethylgallium (TMGa), trimethylindium (TMIn), and ammonia (NH_3) were employed as the reactant sources for gallium, indium, and nitrogen, respectively. CP_2Mg was used as the sources for p-type dopants. For the growth of InN structures, V/III ratio of NH_3 and TMIn was around 2×10^4 during the InN formation process for several minutes. The doping concentration of Mg-doped GaN layer is 5×10^{17} cm^{-3}. After the MOCVD growth, the ALD technique was applied to grow a 200-nm-thick ZnO:Al thin film at a temperature of 200°C. After the growth is done, standard semiconductor fabrication was employed to obtain the photodetector devices. The Cr/Au (30nm/800nm) alloys are used for contact metals. The mesa was defined by dry-etch with the size of 14 mil by 14 mil (355 μm by 355 μm). The schematic diagram of the finished device is depicted in Fig. 1.

Due to its highly volatile nature, the indium element is very difficult to incorporate into the InN film in the MOCVD system. If the substrate temperature is too high, there will be no InN formed. So this situation limits the epitaxial layer design. The basic constraint is the growth temperature must be low after the InN deposition. Following this thought, putting LT-GaN and ZnO on top of InN layer is very suitable for our purpose. First, both of them can take the low temperature deposition. The LT-GaN layer is the last one to be deposited in the MOCVD system and its growth temperature is the same as that of the InN step. The ZnO layer was deposited in the separate ALD system whose growth temperature is controlled at 200°C. The LT-GaN provides the first layer of protection for InN when the wafer was left in the air for transferring to the ALD system. The thicker ZnO layer can provide further protection from environmental erosion and also become the transparent conducting layer for the device.

Because the ZnO layer was deposited separately and the wafers were under such low temperature (200°C), with similar surface material and morphology, we believe the difference of the ZnO materials among these three samples should be minimum. The published paper demonstrated that the optical transmission is the same and the conductivity is close (7.7×10^{-4} vs. 3×10^{-3} Ω•cm) for the ZnO layers deposited on very different substrates (glass and sapphire) [26].

#249488 Received 4 Sep 2015; revised 7 Nov 2015; accepted 16 Nov 2015; published 20 Nov 2015

In this work, three InN samples capped with LT-GaN with different growth temperature (510, 530, 550 degrees Celsius) were made for characterization, and they are named as InN-510, InN-530, and InN-550 for the references in the following texts. The material properties of the InN layer were characterized using field-emission scanning electron microscopy (SEM), and energy dispersive spectroscopy (EDS) taken by a JEOL ARM-200F system, high resolution X-ray diffraction (HRXRD) performed by a PANalytical X'Pert Pro X-ray diffractometer, and photoluminescence (PL) using the 633 nm line of a He-Ne laser as the excitation source. Finally, after normal clean-room processes are finished, the external quantum efficiencies (EQE) measurement was carried out under monochromatic illumination, and a 1000W Class A solar simulator with a xenon lamp and an Air Mass 1.5 Global (AM1.5 G) filter are employed to evaluate current density-voltage (*J-V*) under dark and illumination conditions.

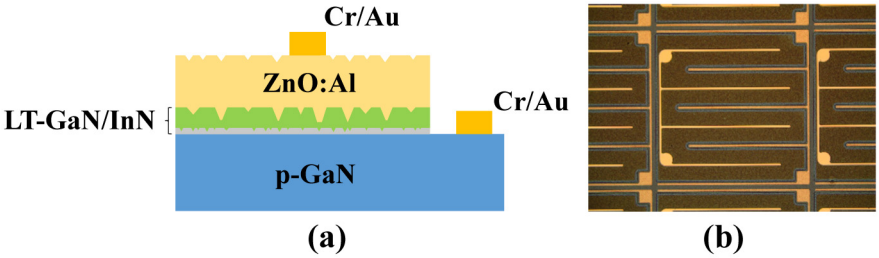

Fig. 1. (a) Schematic of a ZnO/LT-GaN/InN heterojunction photodetection devices. (b) The microscopic image of a finished device under test.

3. Results and discussion

3.1 SEM and EDS characterization

After the wafers were grown, we use SEM system to inspect the surface morphology and cross-sectional images of the samples. In Fig. 2(a), numerous InN islands fill the surface of the wafer. To look closer, the base width of these islands ranges from 50 nm to 250 nm and the height is about 200 nm, as shown in Fig. 2(b). As shown in Fig. 2(c), indium droplets can be seen when the growth temperature reduces to 510°C, and this phenomenon is mainly due to insufficient NH_3 decomposition [16, 27]. Figure 2(d) shows different preferential facet growth when substrate temperature is 550°C or above.

Figures 2(e)–2(h) show the cross-sectional SEM and Energy Dispersion Spectroscopy (EDS) measurements of finished ZnO/LT-GaN/InN layer on the p-GaN:Mg. As shown in the cross-sectional SEM, air voids were observed between the p-GaN buffer layer and the supposed InN layer. Instead of a uniform thin film, the InN layer grown at low temperature looks like nano-scale pyramids spreading through the surface [9]. From the surface and cross-sectional images, the average thickness of these In-rich layer is about 35 nm. Taking the EDS spectrum at various points of this cross-section, as the circled area shown in Fig. 2(e), reveals that the upper layer is solely composed of ZnO, and the layer next to the p-GaN surface (area (h)) has In composition. On the other hand, another spot at similar location (area (g)) exhibits both Ga and In composition. The inter-mixing of In and Ga could rise from the Ga diffusion during the growth and this should be the reason why the voids are formed between In-rich and p-GaN layers [9].

#249488 Received 4 Sep 2015; revised 7 Nov 2015; accepted 16 Nov 2015; published 20 Nov 2015

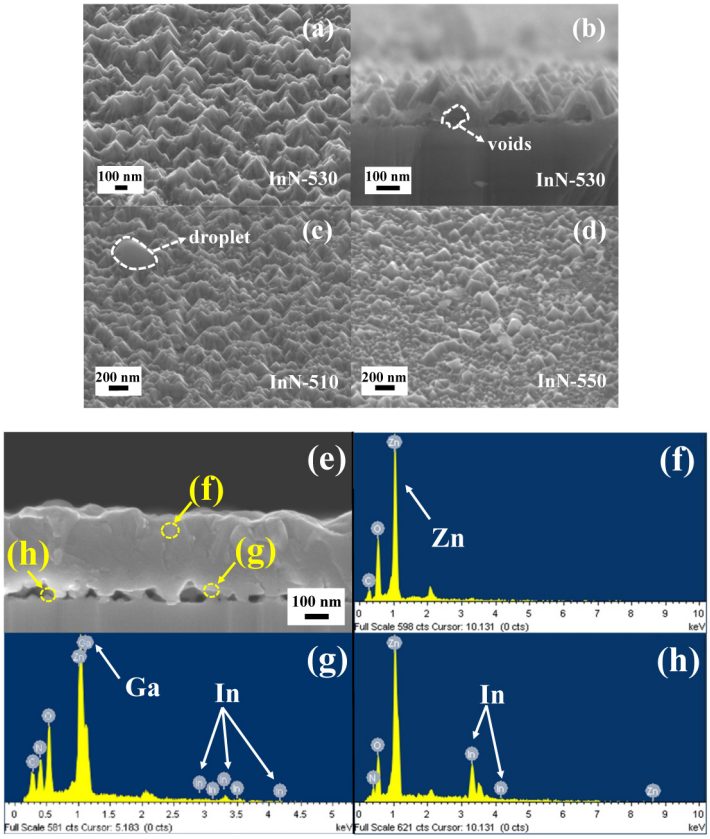

Fig. 2. (a) Bird-view SEM image of InN capped with LT-GaN at growth temperature of 530°C on the GaN substrate. (b) Cross-section SEM image of InN capped with LT-GaN at growth temperature of 530°C. (c) and (d) Bird-view SEM image of InN-510 and InN-550 samples. (e) Cross section-view SEM image of ZnO/LT-GaN/InN on the p-GaN:Mg substrate. The inset f and g symbols indicate the different measured area on the sample. (f), (g), and (h) are the energy dispersive spectrometer (EDS) data.

3.2 X-ray analysis

Another powerful tool to check the grown InN quality is the HRXRD. The samples under the tests were all covered by LT-GaN and InN grown at various temperatures. Figure 3(a) shows the detailed XRD 2-theta scan of the three samples measured by the PANalytical X'Pert Pro X-ray diffractometer. Several pronounced peaks can be observed in this plot: sapphire peak around 42°, GaN (0002) peak at 34.5°, and InN (0002) peak at 31.38°. The sapphire peak around 41° is used as the reference. Since we did not see the fringes pattern around the InN peak, a fully relaxed crystal is assumed. There are some disparities that can be seen in these three samples from this XRD plot. First, when closely inspected, it can be found that the InN-related peak in InN-550 is actually deviated from the real InN peak. When the fully relaxed crystal is assumed, the indium composition can be obtained as 0.92. Between InN(0002) and GaN(0002), a broad band signal indicates the formation of InGaN composite. One particular peak stands out in both InN-550 and InN-510 at 32.9°, and it was identified as the possible peak for In(101) or InN(1-101) [28]. To clarify this confusion, an extended X-ray scan was taken, and no In(110) can be found at 38° which eliminates the possibility of indium existence [28]. Another broad peak can be seen in InN-550 close to GaN peak, and it represents the relaxed $In_{0.25}Ga_{0.75}N$ from the location of the peak.

#249488 Received 4 Sep 2015; revised 7 Nov 2015; accepted 16 Nov 2015; published 20 Nov 2015

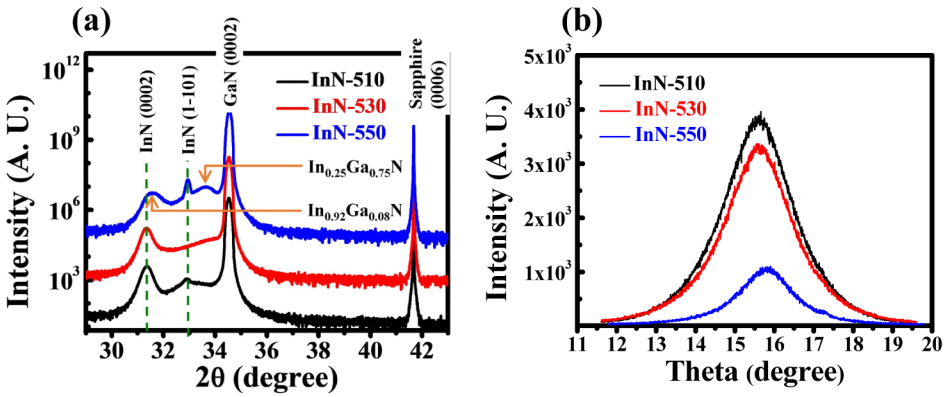

Fig. 3. (a) The X-ray diffraction pattern of a LT-GaN/InN film on GaN at the different growth temperature. (b) The rocking curves of the three samples.

One of the experiments we could perform to check the crystal quality is the rocking curve in X-ray diffraction. Certain types of imperfection of the epitaxial layer, such as mosaicity and dislocations, can broaden the linewidth of the rocking curves. From our rocking curves, shown in Fig. 3(b), the sample linewidths from different growth temperatures (InN-510, InN-530, and InN-550) are 7405, 7005, and 5601 arcsecs, respectively. To compare with previous results, the thickness of the growth, the type of film, the FWHM and the growth method were chosen as the key parameters and summarized in Table 1.

Table 1. The comparison of the rocking curves of InN samples

Thickness (nm)	InN film type	FWHM (arcsec)	Growth Method	Reference
20~60	Nanostructure and film on GaN	5601~7405	MOCVD	Our study
200	Film on Sapphire	3200~9000	PA-MOCVD	[29]
100~200	Film on Sapphire	900~9000	PR-MOVPE	[30]
240~960	Film on GaN	2920~3520	RF-MBE	[31]
5~460	Microstructure to Film on GaN	250~750	RF-MBE	[32]
730~1000	Film on GaN	455~1167	PA-MOMBE	[33]

In Table 1, most of InN materials were grown by plasma-assisted MBE or MOCVD. If the FWHM of the rocking curves can be viewed as an indicator of crystal quality, then, from this table, we could realize that MBE still produces the best quality of InN material to this day. Our InN sample, on the other hand, while seems not very good in terms of broad rocking curves, can still be treated as an average grade because the FWHM of the rocking curve can be seriously affected by the film thickness: as the thickness reduces, the FWHM increases dramatically [34, 35]. Even so, more improvements on MOCVD epitaxial technology are definitely necessary.

3.3 PL analysis

The photoluminescence (PL) was measured using the 633 nm line of a He-Ne laser as the excitation source. Figure 4 shows the PL spectra of InN samples measured at 20 K and room temperature. While InN samples grown at 510°C and 530°C look like single-peaked, all three samples' result can be fitted very well with three individual Gaussian peaks. The room temperature PL intensity of InN samples is about 7~17 times weaker than the 20K measurement. A slightly red-shift of PL peak from 20K to 300K was recorded. A comparison of infrared PL peak intensity under the constant excitation power was shown in Fig. 4(d).

#249488 Received 4 Sep 2015; revised 7 Nov 2015; accepted 16 Nov 2015; published 20 Nov 2015

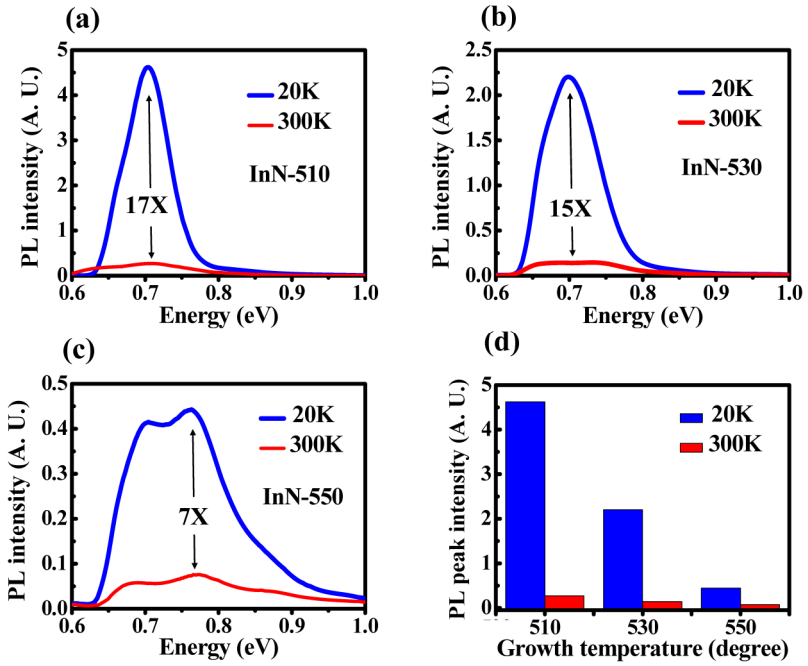

Fig. 4. (a), (b), and (c) Photoluminescence of InN layer under cryogenic and room temperature. (d) PL peak intensity versus growth temperature of InN layers measured at cryogenic and room temperature.

Figures 5(a)–5(d) reveal the individual Gaussian functions that fit the experimental results best for all three cases. The detailed parameters of fitting curves are extracted and listed in Table 2. From the peak position among these data, InN-550 sample shows a global blue-shift and a lower-than-E_g peak shows up in all three cases. If the major peaks at 0.66eV and 0.7eV are kept during the fitting, InN-510 and InN-530 need very little contribution from the third Gaussian (the higher energy one), while the InN-550 takes several more to fulfill the fitting requirement, as can be seen in the Table 2. According to previous scanning transmission electron microscopy (STEM) results, the blue-shift phenomenon of the InN band to band peak with increasing growth temperature could be attributed to the complex $In_xGa_{1-x}N$ formation due to gallium diffusion at higher growth temperature and the loss of pure InN material [9, 36–38]. The 0.66 eV component in the PL spectra can be attributed to the deep acceptor states in InN film [38, 39].

Table 2. The Gaussian Fitting Multiple Peaks of InN Samples with Different Growth Temperature

Sample	InN-510		InN-530		InN-550	
	Energy (eV)	Intensity (a.u.)	Energy (eV)	Intensity (a.u.)	Energy (eV)	Intensity (a.u.)
Peak 1	0.66	0.615	0.66	0.637	0.66	0.071
Peak 2	0.7	4.519	0.7	2.22	0.7	0.38
Peak 3	0.78	0.215	0.8	0.03	0.76	0.31
Peak 4					0.82	0.172
Peak 5					0.95	0.019

#249488 Received 4 Sep 2015; revised 7 Nov 2015; accepted 16 Nov 2015; published 20 Nov 2015

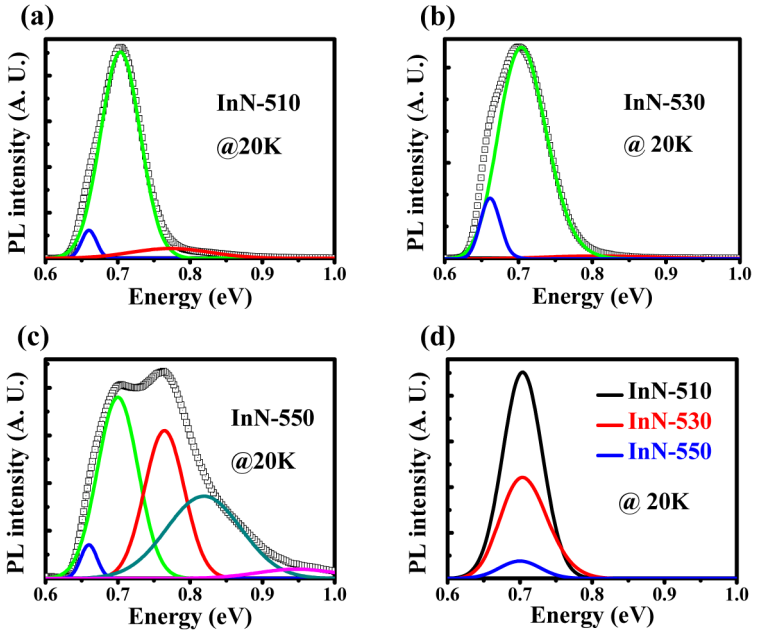

Fig. 5. The photoluminescence spectra at 20 K for (a) InN-510 (b) InN-530 (c) InN-550; Color lines are marked to multiple peaks calculated by Gaussian distribution method. (d) The comparative major Gaussian peak spectra of InN samples excited by a pumped laser power of 4 mW.

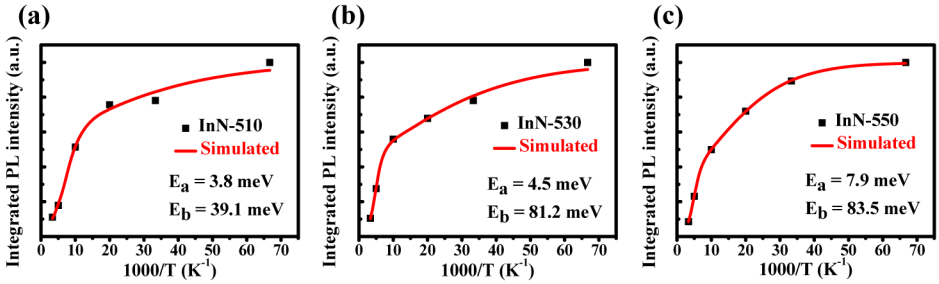

Fig. 6. Variation of the integrated PL intensity with temperature. The solid line is the fit to the data points using Eq. (1).

Another useful information can be obtained from temperature dependent PL. The thermal quenching of the integrated intensities can be understood by the rate equation of the radiative / non-radiative recombination processes. By assuming two different non-radiative processes, the intensity I can be written as [40, 41]:

$$I(T) = \frac{I_0}{\left[1 + A\exp(-\frac{E_a}{K_B T}) + B\exp(-\frac{E_b}{K_B T})\right]}, \quad (1)$$

where $I(T)$ is the integrated PL intensity at temperature T, I_o is the integrated PL intensity at 0 K, the coefficients A and B are the strengths of the thermal quenching processes. E_a and E_b are the activation energies at low temperature and high temperature regions, respectively. The measured and fitted data are shown in Fig. 6 and the activation energies can be evaluated by Eq. (1). As shown in Table 3, the E_a and E_b rise with increasing growth temperature. From previous research of InGaN, the continuous thin layer (QW) and the quantum disk (or

#249488 Received 4 Sep 2015; revised 7 Nov 2015; accepted 16 Nov 2015; published 20 Nov 2015

segment QW by [42]) could exhibit very different behavior in the temperature-dependent PL [38, 42, 43]. For InN nanostructure, the situation is more complicated due to the addition of shallow/deep acceptor states in the band gap [38, 39, 44]. Intermixing of the Ga atoms can cause the blue-shift of peak wavelength in PL. This shift in the peak wavelength and thus the effective band edge can lead to the increasing E_b for higher growth temperature samples [45].

Table 3. The Evaluated Activation Energy Value of InN with Different Growth Temperature

Sample	InN-510	InN-530	InN-550
E_a	3.8 meV	4.5 meV	7.9 meV
E_b	39.1 meV	81.2 meV	83.5 meV

As we just mentioned, the InN situation is more complicated than the ordinary GaN. The usual activation energy calculation in Table 3 might not be totally correct when temperature rises close to 300K. The main problem is the radiative recombination rate is no longer a constant [46–48]. To fully understand the carrier dynamics, the temperature dependent PL need to be analyzed in detail.

In the indium nitride, the residual carrier concentration is usually high if no special attention is taken during the growth (which should be our case). For such so-called "degenerate" InN film or nanostructure, the electron concentration can be very high ($>10^{18}cm^{-3}$) and thus the band diagram in a nanostructure can be like in Fig. 7(a). The Fermi level of the InN film (E_{fn}) is located above the E_c (conduction band minimum) and the Burstein-Moss effect can happen. For the acceptor-like level (E_A) in the band gap, when no specific impurities are inserted, Jenkins, et al., asserted the In vacancy (Va_{In}) can be a very probable candidate [49]. These In vacancies also tends to "cluster" together in the InN film [50], which can lead to the non-uniform distribution of the acceptor level and lead to a situation similar to potential fluctuation [51].

Once the band structure and the acceptor level are drawn, as shown in Fig. 7(a), three different optical transitions can occur: (1) The transition between the electrons close to Fermi level edge and the holes localized on E_A; (2) band to band transition at low k; (3) band to acceptor transition [52]. Because of these three co-existing processes, the analysis of PL spectrum becomes complicated. On the other hand, if we could manage the PL spectra well, a lot of information can be extracted from these results.

In our study, both power and temperature dependent PL were measured. For the power-dependent PL spectra at low and high temperatures (20K and 300K, respectively), our measurements showed almost the same lineshape for low and high excitation power among three samples. The excitation power varied from 0.5mW up to 4mW in these measurements. According to previous analysis of Klochikhin, et al. [39], the PL spectra of the degenerate InN (or the InN with medium to high residual electron concentration) are insensitive towards the excitation power, which can be observed in our results.

#249488 Received 4 Sep 2015; revised 7 Nov 2015; accepted 16 Nov 2015; published 20 Nov 2015

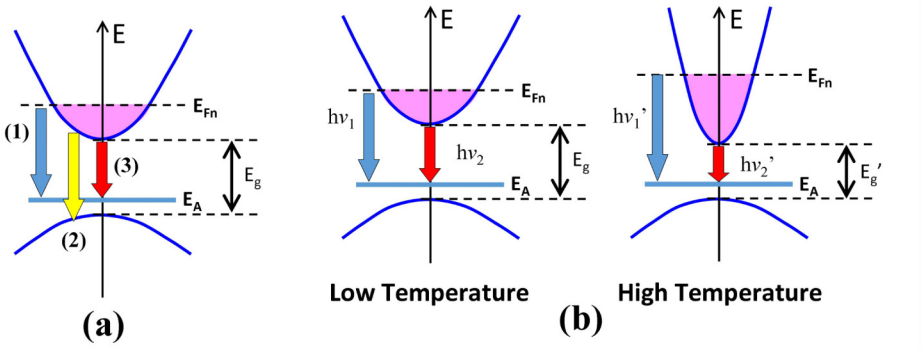

Fig. 7. (a) The optical transitions in the InN. (b) The temperature effect on the InN band structure and optical transition [53].

The band to band transition (2) is usually weak [52], so we can consider the transitions (1) and (3) only. When the temperature rises during the measurement, the effective band gap (Eg becomes Eg') shrinks following the Varshini's law. Meanwhile, the E_{fn} increases so much that the transition (1) can actually have equal or higher photonic energy than before (as shown in Fig. 7) [53]. So when comparing the emission spectrum at low and high temperature, one branch reduces the transition energy (band to acceptor) while the other increases (Fermi-level electron to acceptor state). To verify this conjecture, we must inspect the PL spectra carefully. Since both transitions can exist in our InN layer, it is imperative for us to trace the constituent branches via Gaussian fitting curves. In Fig. 8, the temperature dependent PL spectra of the three samples with different growth temperatures are demonstrated. All the data were normalized to the individual maximum to reveal the detailed features in lineshapes. Even at 15K, the FWHM of the spectra is generally wider because there are two major peaks combined inside the PL spectrum. Once the temperature started to rise, these two branches moved towards different directions. As a consequence, both InN-510 and InN-530 evolved into even broader spectra at room temperature and the two peaks are about 66meV apart. For InN-550, the situation is similar, and the residual carrier seems to be more than the other two cases, so the Fermi-level to acceptor transition sits around 0.77eV due to the Burstein-Moss effect and this peak is quite insensitive to temperature variation. However, the other lower energy peak at 0.66eV red-shifted like the InN-510 and InN-530 did, and the quantity of the shift is also about the same among these three samples, which could be viewed as an indicator of the universal InN band gap shrinkage.

From the past literatures, the InN samples with low residual carrier concentration can reveal the acceptor state structures [39], and the binding energies of these acceptor states can be correlated to the activation energies of the recombination channels [54]. If there are two recombination channels, usually one for shallow and one for deep acceptor states, and their activation energies are 5-10meV and 50-80meV, respectively [39, 44, 51]. Our findings in Table 3 agree with these numbers quite well. Although the radiative recombination time is usually set to be constant in these papers, a more detailed study on the TRPL and non-radiative recombination time will be necessary.

#249488 Received 4 Sep 2015; revised 7 Nov 2015; accepted 16 Nov 2015; published 20 Nov 2015

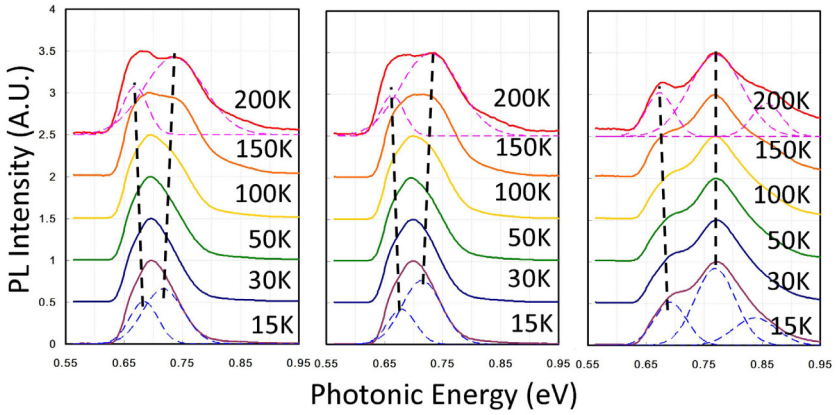

Fig. 8. The temperature dependent PL spectra for three samples. All the PL spectra were normalized to theirs.

3.4 Photodetector characterization

After material characterization, the properties of the ZnO/LT-GaN/InN photodetectors were tested. The narrow band gap of InN provides a unique opportunity for infrared photon detection in the nitride-based devices. The InN-530 was chosen as the main active material for device fabrication because of its strong PL intensity and good X-ray diffraction result. The other feature of this combination is in the band alignment. The band alignment between GaN and ZnO is a type-II junction and when the InN layer is inserted, the band diagram similar to the double-heterostructure, which is preferred in most optoelectronic devices, can be expected [55, 56]. Figure 9(a) and 9(b) show the band diagram of the ZnO/LT-GaN/InN structure under zero and −2V calculated by APSYS. In our current doping design, most of the voltage drops fall at the InN/GaN interface, which is not preferable for carrier extraction and could be one of the reasons leading to low quantum efficiency. Further optimization is necessary to find the best doping scheme.

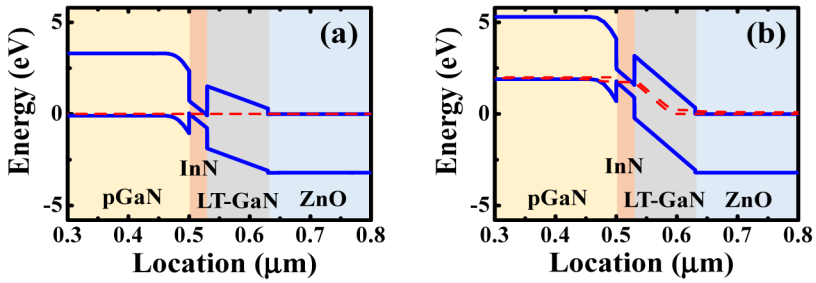

Fig. 9. The calculated band diagram of a ZnO/LT-GaN/InN structure. (a) Zero bias, (b) Negative bias of 2V. The red dotted line is the Fermi level (or Quasi-Fermi level at −2V).

To evaluate photodetection capability of the device, two different types of measurements were made: one is the photovoltaic response and the other is the external quantum efficiency of the device. Figure 10(a) reveals the *J-V* characteristics under dark and AM1.5G illumination conditions, and Fig. 10(b) shows the external quantum efficiencies (EQE) of the InN photodetector at the reverse bias of 0, 3 and 7 Volts. The efficiencies are peaked at the wavelength of 1770 nm. Both results at −3 and −7 volts show the same up-rising trend towards the longer wavelength, and the EQE value as high as 3.55% is recorded. Similar oscillating pattern can be observed in the long wavelength section of the EQE spectra from different bias. Based on our simulation, this is originated from the Fabry-Perot effect between

#249488 Received 4 Sep 2015; revised 7 Nov 2015; accepted 16 Nov 2015; published 20 Nov 2015

the sapphire substrate and the thick InN/GaN structure above. Strong photoresponse under solar simulator rises from absorption in both p-GaN and InN layers. Combining the photo-current and EQE measurement (Fig. 10(a) and 10(b)), one can calculate the portion of photocurrents in Fig. 10(a) that are brought by InN layer by the following formula:

$$\frac{Photocurrent\ from\ InN\ at\ reverse\ bias}{Total\ photocurrent\ measured\ at\ reverse\ bias} = \frac{q\int_{800nm}^{1800nm} F(\lambda)\times EQE(\lambda)d\lambda}{q\int_{Total} F(\lambda)\times EQE(\lambda)d\lambda}, \quad (2)$$

where I_{photo} is the measured photocurrent, $EQE(\lambda)$ is the EQE spectrum in Fig. 10(b), and $F(\lambda)$ is the standard AM1.5G solar spectrum. As high as 7.80% of the I_{photo} can be attributed to InN contribution at reverse bias of 0.3V. From the *J-V* curves and EQE spectrum, there is no so-called "short-circuit current" at zero bias for our devices, which indicates no carrier extraction without external electrical field possibly due to traps and defects formation in the materials. Currently the growth of the InN layer still needs optimization as the possible defects cause extra loss and inefficient photo-response. Meanwhile, the InN layer sandwiched by ZnO and GaN should be regarded as a promising candidate for infrared photonic applications because of its compatibility in the device growth and possibility to operate beyond the visible-wavelength regime.

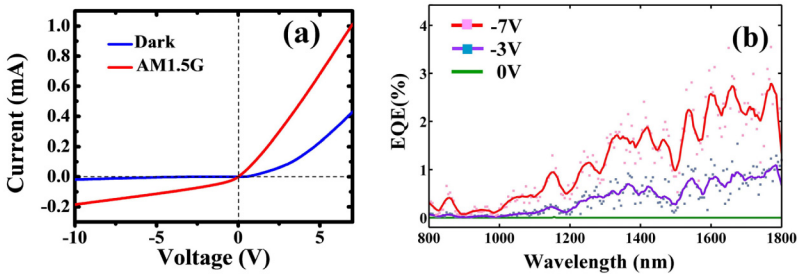

Fig. 10. (a) The plot is the generic *J-V* characteristics of a photodetector under dark and simulated AM1.5G illumination. (b) The measured EQE spectra of the InN device for zero bias and reverse bias. The solid curves are the moving average of the data points.

4. Conclusion

In summary, a ZnO/LT-GaN/InN/p-GaN heterojunction photodiode is demonstrated with extended IR response. The best quantum efficiency is 3.55% and the variation of the growth temperature was used to optimize the InN growth. The current technology and design still have some room to improve. In addition to the InN material quality improvement, the device architecture can be modified to utilize the special characteristics of InN. One of them is the n+/N heterojunction photodetector [9, 10, 57], which can avoid the bad surface of p-GaN, and many groups have reported encouraging results in the past. The combination of such material systems should be promising for the future generation of nitride-based optoelectronic devices because of the unique long-wavelength capability.

Acknowledgment

The work was supported by the National Science Council of Taiwan through the contracts: NSC 101-2221-E-009-046-MY3, MOST 104-2628-E-009-013-MY3, and NSC 102-3113-E-005- 001.

#249488 Received 4 Sep 2015; revised 7 Nov 2015; accepted 16 Nov 2015; published 20 Nov 2015